Supplementary Information

Ultrafine low loading AgCu nanoclusters supported on defective ZIF-8 for click reaction with high stability

Xinghao Li,[a,b] Sara Ajmal,[a] Penghui Fang,[a,b] Xiaoxing Zhou,[a,b] Maoni Lu,[a,b] Sichen Li, [a,b] Ping Chen,[a] Peng Li,[*a,b] and Manzhou Zhu[a,b]

[a] Department of Chemistry and Center for Atomic Engineering of Advanced Materials, School of Materials Science and Engineering, Anhui Province Key Laboratory of Chemistry for Inorganic/Organic Hybrid Functionalized Materials, Anhui University, Hefei 230601, China.

[b] Key Laboratory of Structure and Functional Regulation of Hybrid Materials, Ministry of Education, Anhui University, Hefei 230601, P. R. China.

* Email: peng-li@ahu.edu.cn

1. Additional experiment details

1.1 Characterization method

The UV-visible spectra were recorded by a Techcomp UV1000 spectrophotometer. The transmission electron microscope (TEM) images, X-ray spectrometer (EDS), and high-angle annular dark-field scanning TEM (HAADF-STEM) were performed on the Tecnai TF-20. The Fourier transform infrared (FT-IR) spectra were recorded with the Bruker Tensor 27 instrument. The Power X-ray diffraction (XRD) patterns were collected on a Smart Lab 9 KW with Cu Kα radiation. The X-ray photoelectron spectroscopy (XPS) measurements were conducted on ESCALAB 250. The content of elements was determined using an inductively coupled plasma emission spectrometer. The X-ray absorption fine spectrum (XAFS) was recorded on Table XAFS-500 (Specreation Instruments Co., Ltd., China). The electron paramagnetic resonance (EPR) was tested on Bruker EMX nano spectrometer.

1.2 Preparation D-ZIF-8

Synthesis was carried out following the procedure described in the previous literature on ZIF-8.[1] Then, ZIF-8 (300 mg) was calcined at 300 ℃ under nitrogen atmosphere for 3 hours with a heating rate of 5 ℃/min, and subsequently cooled to room temperature to obtain defective ZIF-8 (denoted as D-ZIF-8).

1.3 Synthesis of the AgCu/D-ZIF-8-X catalysts (X is heat treatment temperature of AgCu/D-ZIF-8, X=120, 260, 500 ℃)

AgCu/D-ZIF-8 (100 mg) was calcined in a vacuum tube furnace with nitrogen atmosphere at 120 ℃ for 2 h (heating speed: 5 ℃/min) and then cooled to room

temperature to obtain AgCu/D-ZIF-8-120 catalysts. Using the same method, the AgCu/D-ZIF-8-260, AgCu/D-ZIF-8-500 catalysts were obtained at 260 ℃ and 500 ℃, respectively.

1.4 Synthesis of $Cu_{25}H_{22}((p\text{-}FPh)_3P)_{12}$ nanocluster

The $Cu_{25}H_{22}((p\text{-}FPh)_3P)_{12}$ was obtained via the previously reported.[2] Initially, 180 mg Cupric(II) acetylacetonate was dissolved in 13 mL CH_3OH and added to a 100 mL round bottom flask. Then, 38 mL CH_2Cl_2 was added to the above solution. The solution was stirred in a 36 ℃ oil bath. After vigorous stirring for 30 minutes, 300 mg $(p\text{-}FPh)_3P$ was rapidly added to above solution. The color of the reaction solution became light blue. Following this, 2 mL of $NaBH_4$ (75 mg/mL) dissolved in deionized water was added, gradually causing the color of solution to change to light brown with 1 hour. The reaction proceeded with stirring for 5 hours to obtain the $Cu_{25}H_{22}((p\text{-}FPh)_3P)_{12}$ nanocluster.

1.5 Synthesis of Ag_{25} nanocluster

The Ag_{25} nanocluster was obtained via the previous literature.[3] 0.038 g of $AgNO_3$ was dissolved in 2 mL of methanol and added to 15 mL of dichloromethane solvent. Subsequently, 90 µL of 2,4-dimethylphenylthiol was added to the above mixture solvent. After stirring in an ice bath for 30 minutes, 0.006 g of tetraphenylphosphonium bromide in a methanol solution (0.5 mL) was added and stirred for 30 minutes. Then, the ice-cold aqueous $NaBH_4$ (15 mg/mL) was added to the above solvent, followed by continued stirring for 6 hours under an ice bath. Finally, the nanoclusters in the mixture reaction were washed with methanol and

extracted with CH_2Cl_2 to obtain the pure nanoclusters.

1.6 Synthesis of $Ag_{30}Cu_{14}(TPP)_4(SR)_{28}$ nanocluster

The $Ag_{30}Cu_{14}(TPP)_4(SR)_{28}$ nanocluster was prepared via the previous literature.[4] 0.03 g $AgNO_3$ and 0.06 g of TPP were dissolved in 6 mL of ethanol and then transferred the solution to a 50 mL round bottom flask to form a colorless solution. After stirring for 5 minutes, 0.42 mmol of 3-methylene thiol and 0.034 g $CuCl_2{\cdot}H_2O$ were sequentially added to the above mixture solution. Following an additional reaction time of 10 minutes, the solution was centrifuged to obtain the white precipitation. Simultaneously, the supernatant containing excess ligands was discarded. The obtained white precipitate was then dispersed in a mixed solution comprising ethanol and dichloromethane. Subsequently, 2 mL ethanol solution of $NaBH_4$ (0.015 g/mL) was added drop by drop. The color of the mixture changed from white to grey and ultimately to dark brown. After continuing stirring for 6 hours, the reaction mixture was centrifuged to obtain the precipitation of $Ag_{30}Cu_{14}(TPP)_4(SR)_{28}$ nanocluster.

1.7 Synthesis of $(^nBu_4N)_4[Ag_{28}Cu_{12}(SR)_{24}]$ nanocluster

The $(^nBu_4N)_4[Ag_{28}Cu_{12}(SR)_{24}]$ nanocluster was obtained via the previous literature.[5] In an ice bath, $AgNO_3$ (0.01 g) dissolved in 2 mL of methanol was added to a 50 mL round-bottom flask. Subsequently, 0.08 g of CuCl in 10 mL CH_2Cl_2 was introduced, and the mixture was stirred violently. Subsequently, 10 μL of 2,4-dichlorophenyl thiol and 0.06 g of tetrabutylammonium bromide were added. After stirring for 20 minutes, 0.04 g $NaBH_4$ (dissolved in 1 mL of aqueous) and 50 μL of triethylamine

were sequentially added to the reaction mixture. The stirring was continued for 12 hours at 0 ℃. Upon completion of the reaction, the aqueous phase was removed and evaporated for further analysis. The high purity $(^{n}Bu_4N)_4[Ag_{28}Cu_{12}(SR)_{24}]$ nanoclusters were obtained after washing three times with deionized water and dichloromethane.

1.8 Typical steps of the click reaction

The catalytic performance of AgCu/D-ZIF-8 catalysts for click reaction was evaluated. The AgCu/D-ZIF-8 catalysts (40 mg, 0.387wt.% of AgCu loading) were added to a 10 mL reaction tube, followed by the addition of deionized water (2 mL), phenylacetylene (0.30 mmol) and benzyl azide (0.27 mmol). The reaction mixture was stirred at 35 ℃ under argon protection for 12 hours. Subsequently, after the reaction was stopped, the catalysts and the reaction solution were separated through centrifugation. The catalysts were washed three times with dichloromethane. Then, the AgCu/D-ZIF-8 catalysts were dried in vacuum at 60 ℃ for reserve. The reaction solution was extracted with dichloromethane. Ultimately, the yield of target product was determined via GC analysis.

2. Additional Figure and tables

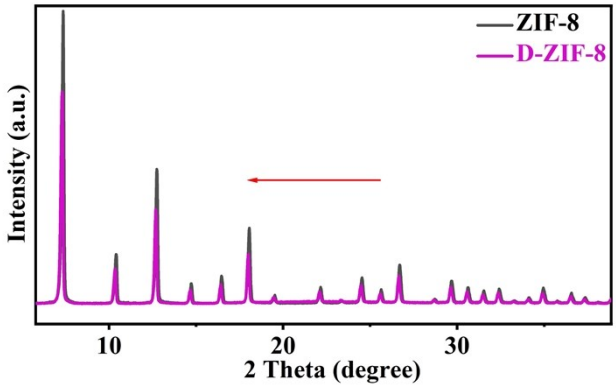

Fig. S1 XRD patterns of ZIF-8 and D-ZIF-8.

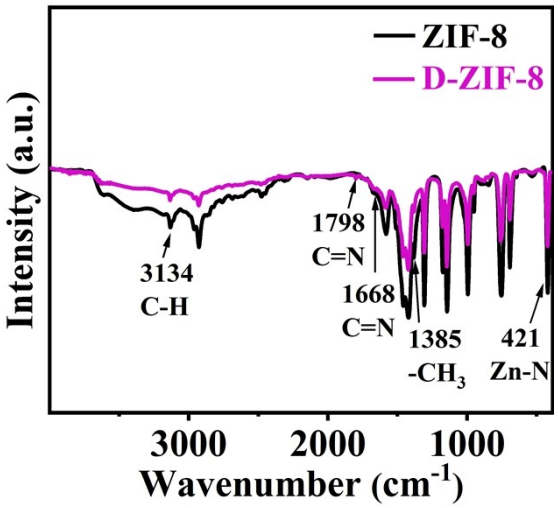

Fig. S2 FT-IR spectra of ZIF-8 and D-ZIF-8.

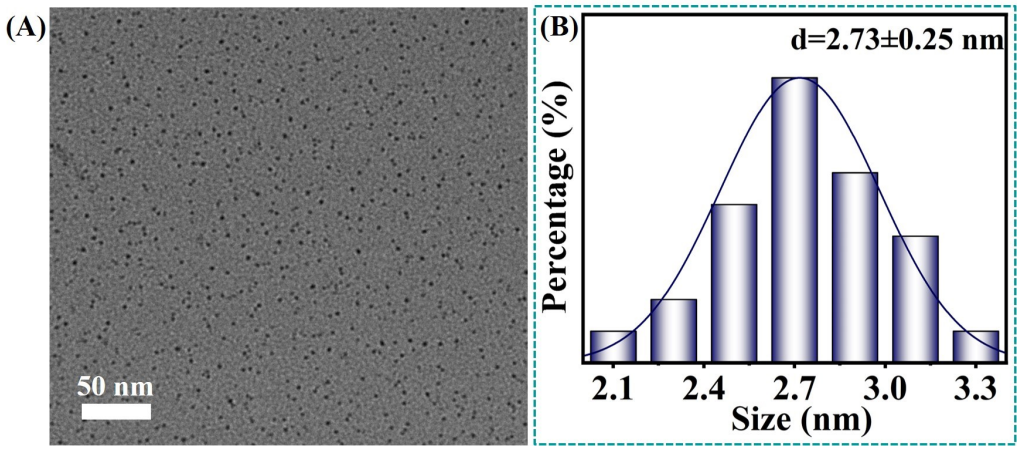

Fig. S3 (A) TEM of AgCu nanoclusters. (B) The size histogram of the AgCu nanoclusters.

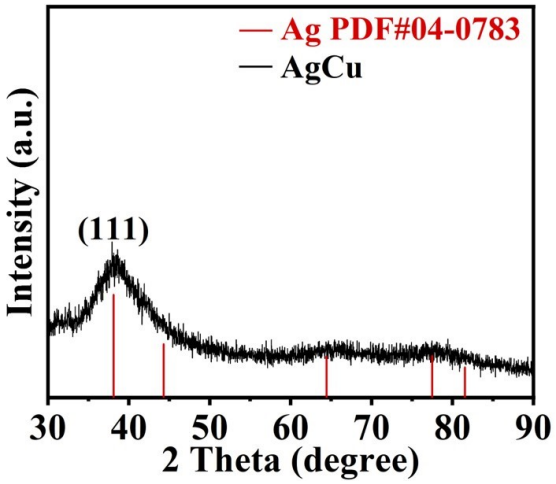

Fig. S4 XRD pattern of AgCu nanoclusters.

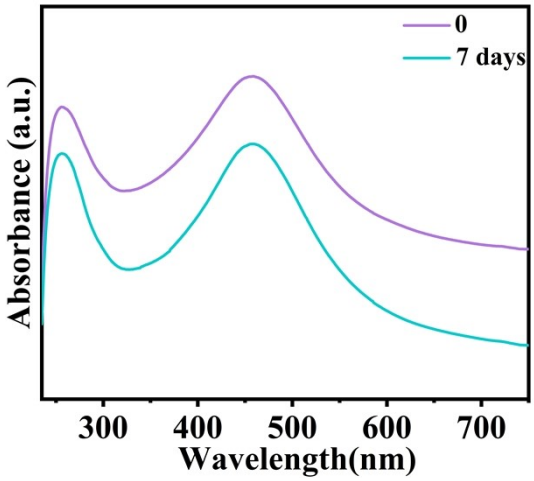

Fig. S5 Time-dependent UV-vis absorption spectra of AgCu nanoclusters in the air atmosphere.

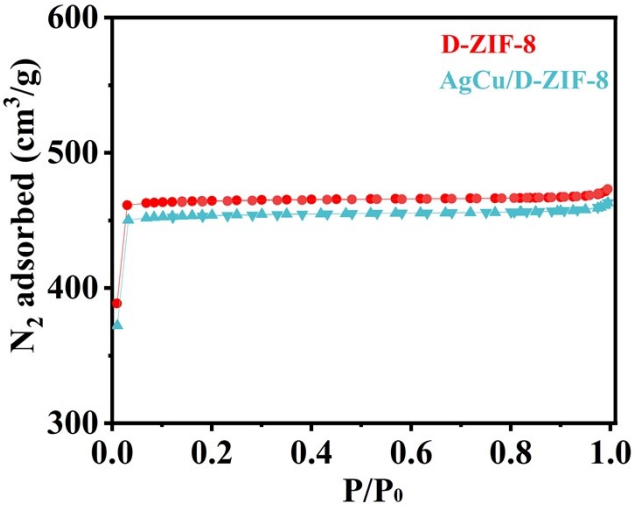

Fig. S6 N_2 adsorption-desorption isotherms of D-ZIF-8 and AgCu/D-ZIF-8.

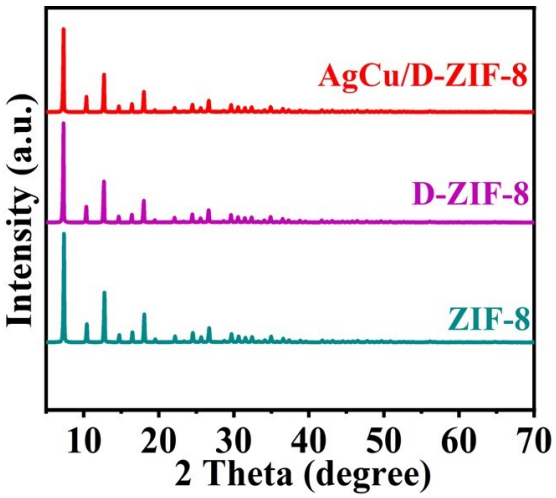

Fig. S7 XRD patterns of ZIF-8, D-ZIF-8 and AgCu/D-ZIF-8 catalysts.

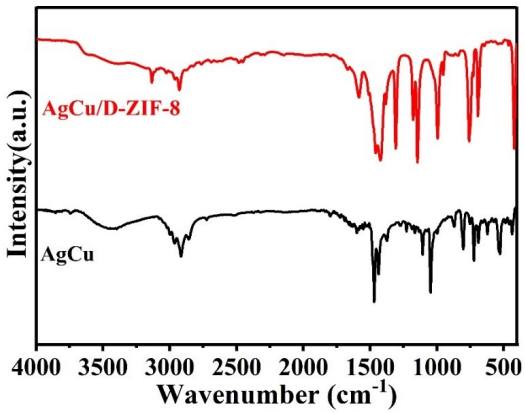

Fig. S8 FT-IR spectra of AgCu nanoclusters and AgCu/D-ZIF-8 catalysts.

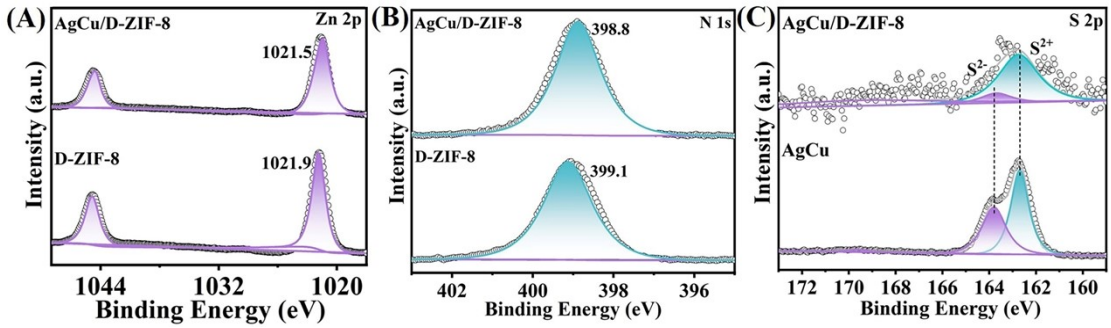

Fig. S9 (A) Zn 2p of D-ZIF-8 and AgCu/D-ZIF-8 catalysts; (B) N 1s of AgCu/D-ZIF-8 and D-ZIF-8. (C) S 2p of AgCu nanoclusters and AgCu/D-ZIF-8 catalysts.

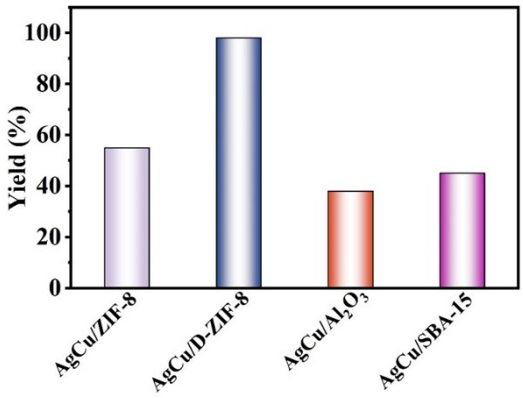

Fig. S10 The yield of catalysts with different supports.

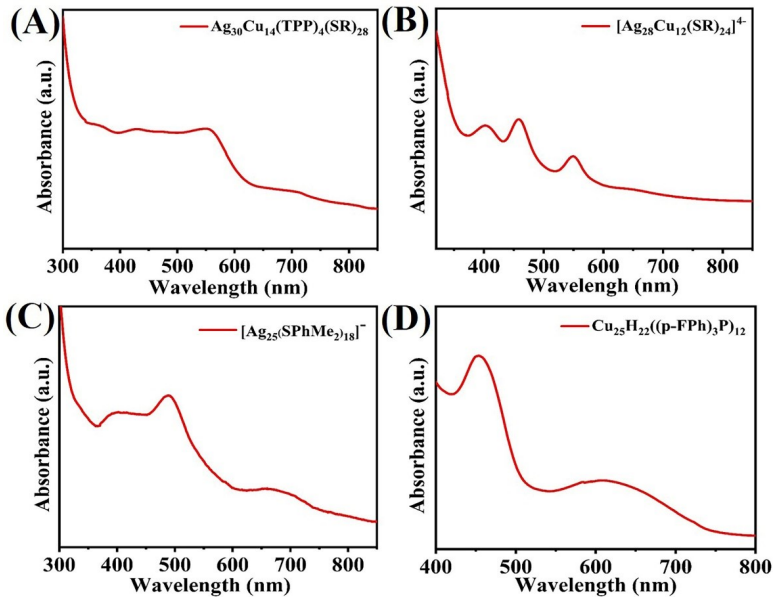

Fig. S11 The UV-vis. spectra of different nanoclusters: (A) $Ag_{30}Cu_{14}$ nanocluster, (B) $Ag_{28}Cu_{12}$ nanocluster, (C) Ag_{25} nanocluster, (D) Cu_{25} nanocluster.

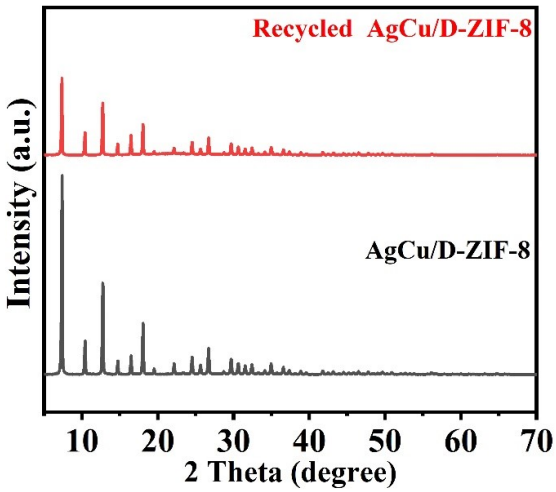

Fig. S12 XRD patterns of AgCu/D-ZIF-8 and recycled AgCu/D-ZIF-8 catalysts.

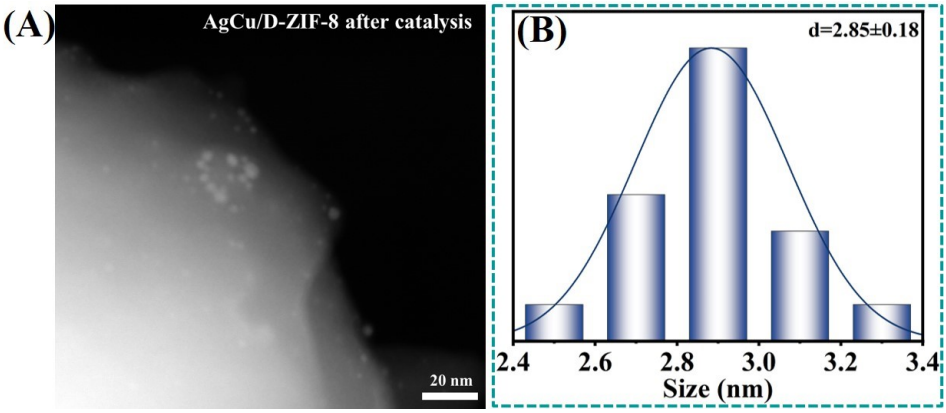

Fig. S13 (A) The TEM image of AgCu/D-ZIF-8 after catalysis. (B) The size histogram of the AgCu nanoclusters in AgCu/D-ZIF-8 catalysts after catalysis.

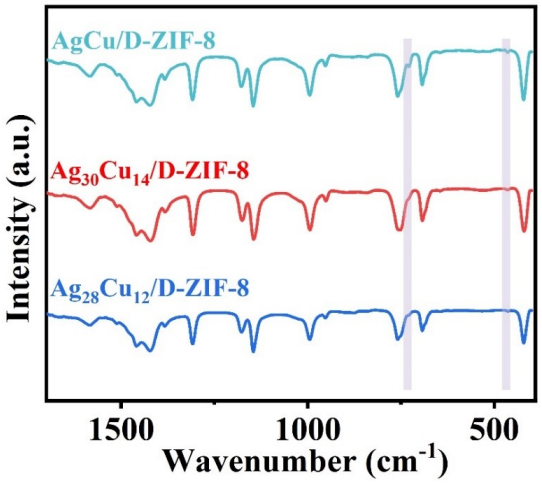

Fig. S14 FT-IR spectra of AgCu/D-ZIF-8, $Ag_{30}Cu_{14}$/D-ZIF-8 and $Ag_{28}Cu_{12}$/D-ZIF-8 catalysts.

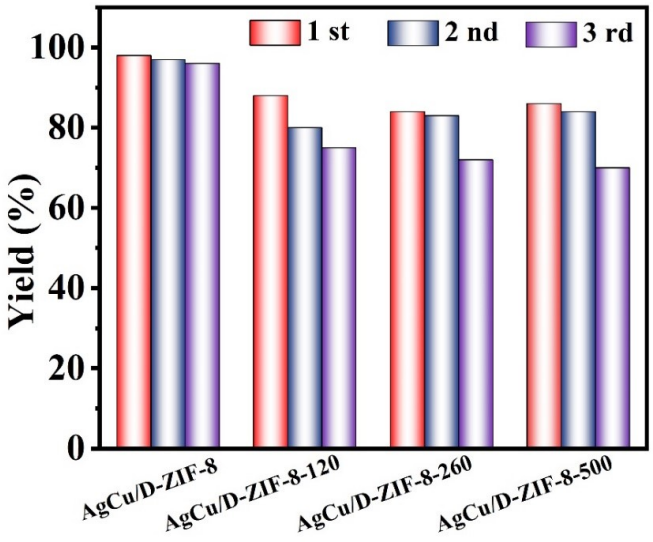

Fig. S15 Recycling experiment of the AgCu/D-ZIF-8, AgCu/D-ZIF-8-120, AgCu/D-ZIF-8-260, and AgCu/D-ZIF-8-500 catalysts.

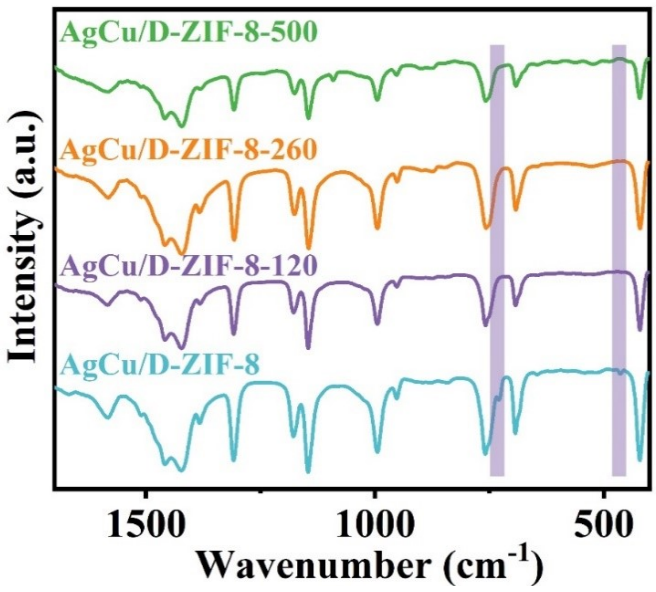

Fig. S16 FT-IR spectra of AgCu/D-ZIF-8, AgCu/D-ZIF-8-120, AgCu/D-ZIF-8-260 and AgCu/D-ZIF-8-500 catalysts.

Table S1 Textural properties of D-ZIF-8, AgCu/D-ZIF-8 and Recycled AgCu/D-ZIF-8.

Sample	D-ZIF-8	AgCu/D-ZIF-8	Recycled AgCu/D-ZIF-8
Surface area (m^2/g)	1294.4	1265.1	1308.2
Micropore area (m^2/g)	1270.3	1239.5	1284.8
Micropore volume (cm^3/g)	0.7079	0.6907	0.6721
Total pore Volume (cm^3/g)	0.7317	0.7161	0.6996
Pore size (nm)	2.2611	2.2643	2.1389

Table S2. The performance of different catalysts to catalyze click reactions.

Entry	Catalysts	Temperature(℃)	Solvent	Yield(%)
1	AgCu	35	H_2O	45
2	D-ZIF-8	35	H_2O	5
3	AgCu/ZIF-8	35	H_2O	54
4	AgCu/D-ZIF-8	40	H_2O	98
5	AgCu/D-ZIF-8	35	H_2O	98
6	AgCu/D-ZIF-8^{9th}	35	H_2O	91
7	$Ag_{30}Cu_{14}$/D-ZIF-8	35	H_2O	85
8	$Ag_{28}Cu_{12}$/D-ZIF-8	35	H_2O	60
9	Cu_{25}/D-ZIF-8	35	H_2O	66
10	Ag_{25}/D-ZIF-8	35	H_2O	/

Table S3. The comparison for click reaction with other reported catalysts.

Entry	Catalysts	Reaction conditions	Yield (%)	Reference
1	Au@Cu nanocubes	H_2O, 50℃	91	6
2	AuCuNWS membrane	EtOH, rt	97	7
3	AuCu	H_2O, 30℃	70	8
4	CuNPs-3 mM-60°C	H_2O, 70℃	90	9
5	SBA-15-Tz-Ru(Ⅱ)TPP	H_2O, 90℃	88	10
6	saCu-2@mpgC_3N_4	H_2O/DMF, 130℃	45	11
7	saCu@nanoC	CH_3CN, 25℃	98	12
8	CuINPs@CFG	H_2O, 70℃	99	13
9	**AgCu/D-ZIF-8**	**H_2O, 35℃**	**98**	**This work**

NMR data of the products

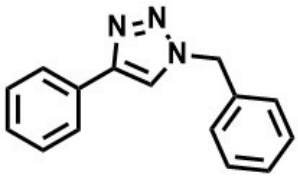

1-benzyl-4-phenyl-1*H*-1,2,3-triazole

^{1}H NMR (400 MHz, $CDCl_3$) δ 7.78 (d, J=8.0 Hz, 2H), 7.65 (s, 1H), 7.40~7.37 (m, 5H), 7.31~7.25 (m, 3H), 5.57 (s, 2H); ^{13}C NMR (101 MHz, $CDCl_3$) δ 148.34, 134.77, 130.62, 129.25, 128.89, 128.89, 128.26, 128.16, 125.79, 119.55, 54.33 ppm.

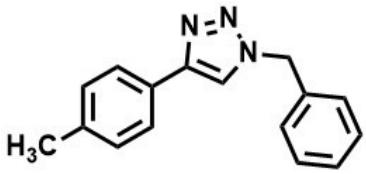

1-benzyl-4-(p-tolyl)-1*H*-1,2,3-triazole

^{1}H NMR (400 MHz, $CDCl_3$) δ 7.67 (d, J=8.0 Hz, 2H), 7.60 (s, 1H), 7.38~7.29 (m, 5H), 7.25~7.18 (d, J=8.0 Hz, 2H), 5.56 (s, 2H), 2.35 (s, 3H) ppm; ^{13}C NMR (101 MHz, $CDCl_3$) δ 148.42, 138.09, 134.84, 129.56, 129.23, 128.85, 128.15, 127.82, 125.70, 119.20, 54.29, 21.35 ppm.

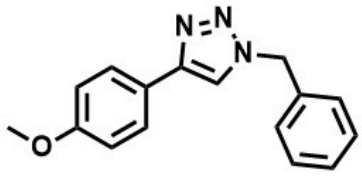

1-benzyl-4-(4-methoxyphenyl)-1*H*-1,2,3-triazole

^{1}H NMR (400 MHz， $CDCl_3$) δ 7.71 (d, J=8 Hz, 2H), 7.56 (s, 1H), 7.38~7.25 (m, 5H), 6.93~6.91 (d, 12Hz, 2H), 5.55 (s,2H), 3.82 (s, 3H) ppm; ^{13}C NMR (101 MHz, $CDCl_3$) δ 159.70, 134.87, 129.23, 128.84, 128.14, 127.10, 123.38, 114.30, 55.40, 54.28 ppm.

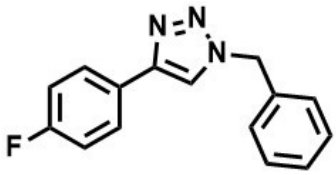

1-benzyl-4-(4-fluorophenyl)-1*H*-1,2,3-triazole

^{1}H NMR (400 MHz, $CDCl_3$) δ 7.77~7.74 (m, 2H), 7.60 (s, 1H) 7.39~7.37 (m,3H), 7.31~7.25 (m, 2H), 7.07~7.05 (t, J=8 Hz, 2H), 5.56 (s, 2H) ppm; ^{13}C NMR (101 MHz, $CDCl_3$) δ 163.99, 161.58, 147. 48, 134.68, 129.28, 128.94, 128.18, 127.57, 127.49, 126.85, 126.82, 119.29, 115.98, 115.76, 54.36 ppm.

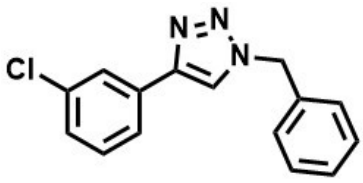

1-benzyl-4-(3-chlorophenyl)-1*H*-1,2,3-triazole

^{1}H NMR (400 MHz, $CDCl_3$) δ 7.77 (m,1H), 7.68~7.66 (m,1H), 7.64 (s,1H), 7.40~7.21 (m,7H), 5.56 (s,1H) ppm; ^{13}C NMR (101 MHz, $CDCl_3$) δ 146.86, 142.53, 134.66, 134.34, 132.21, 129.99, 129.12, 128.81, 128.02, 125.66, 123.65, 119.70, 54.23 ppm.

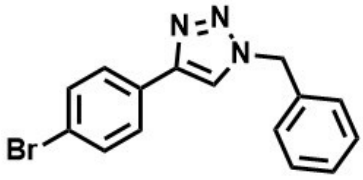

1-benzyl-4-(4-bromophenyl)-1*H*-1,2,3-triazole

^{1}H NMR (400 MHz, $CDCl_3$) δ 7.61~7.59 (m, 3H), 7.57~7.46 (m, 2H), 7.44~7.28 (m, 5H), 5.50 (s, 2H) ppm; ^{13}C NMR (101 MHz, $CDCl_3$) δ 149.72, 134.48, 131.94, 129.51, 129.21, 128.89, 128.11, 127.21, 122.04, 119.50, 54.31 ppm.

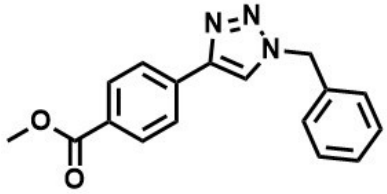

Methyl 4-(1-benzyl-1 *H*-1,2,3-triazol-4-yl)benzoate

^{1}H NMR (400 MHz, $CDCl_3$) δ 8.06~8.05 (d, *J* = 12 Hz, 2H), 7.87~7.85 (d, *J* = 12 Hz, 2H), 7.73 (s, 1H), 7.39~7.25 (m, 5H), 5.56 (s, 2H), 3.90 (s, 3H) ppm. ^{13}C NMR (101 MHz, $CDCl_3$) δ 166.86, 155.01, 147.30, 134.93, 134.51, 132.18, 130.28, 129.68, 129.33, 129.03, 128.23, 125.55, 120.43, 54.91, 51.59 ppm.

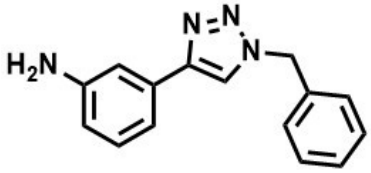

3-(1-benzyl-1*H*-1,2,3-triazol-4-yl)aniline

^{1}H NMR (400 MHz, $CDCl_3$) δ 7.59 (s, 1H), 7.38~7.36 (d, *J* = 7.4 Hz, 3H), 7.29~7.28 (m, 2H), 7.22 (s, 1H), 7.17~7.15 (t, *J* = 7.7 Hz, 1H), 7.09~7.07 (d, *J* = 7.8 Hz, 1H), 6.64~6.62 (d, *J* = 7.8 Hz, 1H), 5.55 (s, 2H), 3.68 (s, 2H) ppm. ^{13}C NMR (101 MHz, $CDCl_3$) δ 148.41, 146.94, 134.81, 131.55, 129.82, 129.24, 128.85, 128.14, 119.62, 116.12, 115.02, 112.31, 54.29 ppm.

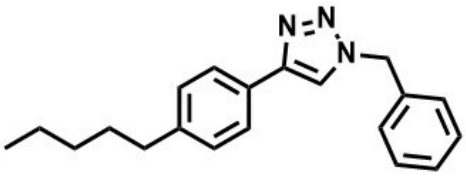

1-benzyl-4-(4-pentylpenyl)-1*H*-1,2,3-triazole

^{1}H NMR (400 MHz, Chloroform-*d*) δ 7.69 (s, 2H), 7.60 (s, 1H), 7.38 (d, *J* = 6.8 Hz, 3H), 7.28 (d, *J* = 7.6 Hz, 2H), 7.20 (d, *J* = 8.0 Hz, 2H), 5.56 (s, 2H), 2.62~2.58 (s, 2H), 1.64~1.58 (s, 2H), 1.31~1.25 (s, 4H), 0.89~0.87 (s, 3H) ppm. ^{13}C NMR (101 MHz, $CDCl_3$) δ 148.46, 143.20, 134.87, 129.23, 128.93, 128.83, 128.12, 128.02, 125.70, 119.22, 54.28 ppm.

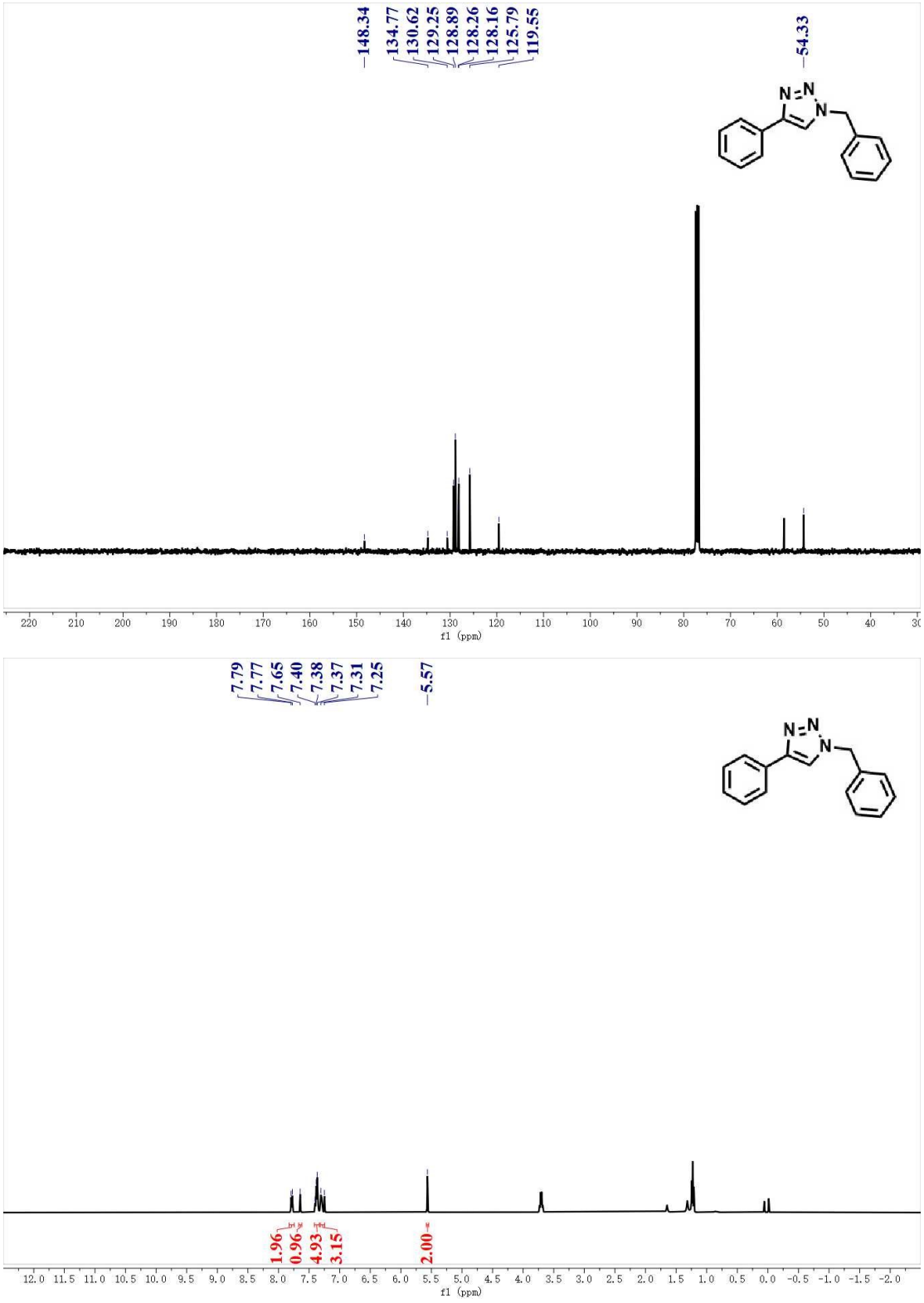

^{1}H and ^{13}C NMR spectra of 1-benzyl-4-phenyl-1*H*-1,2,3-triazole (in $CDCl_3$).

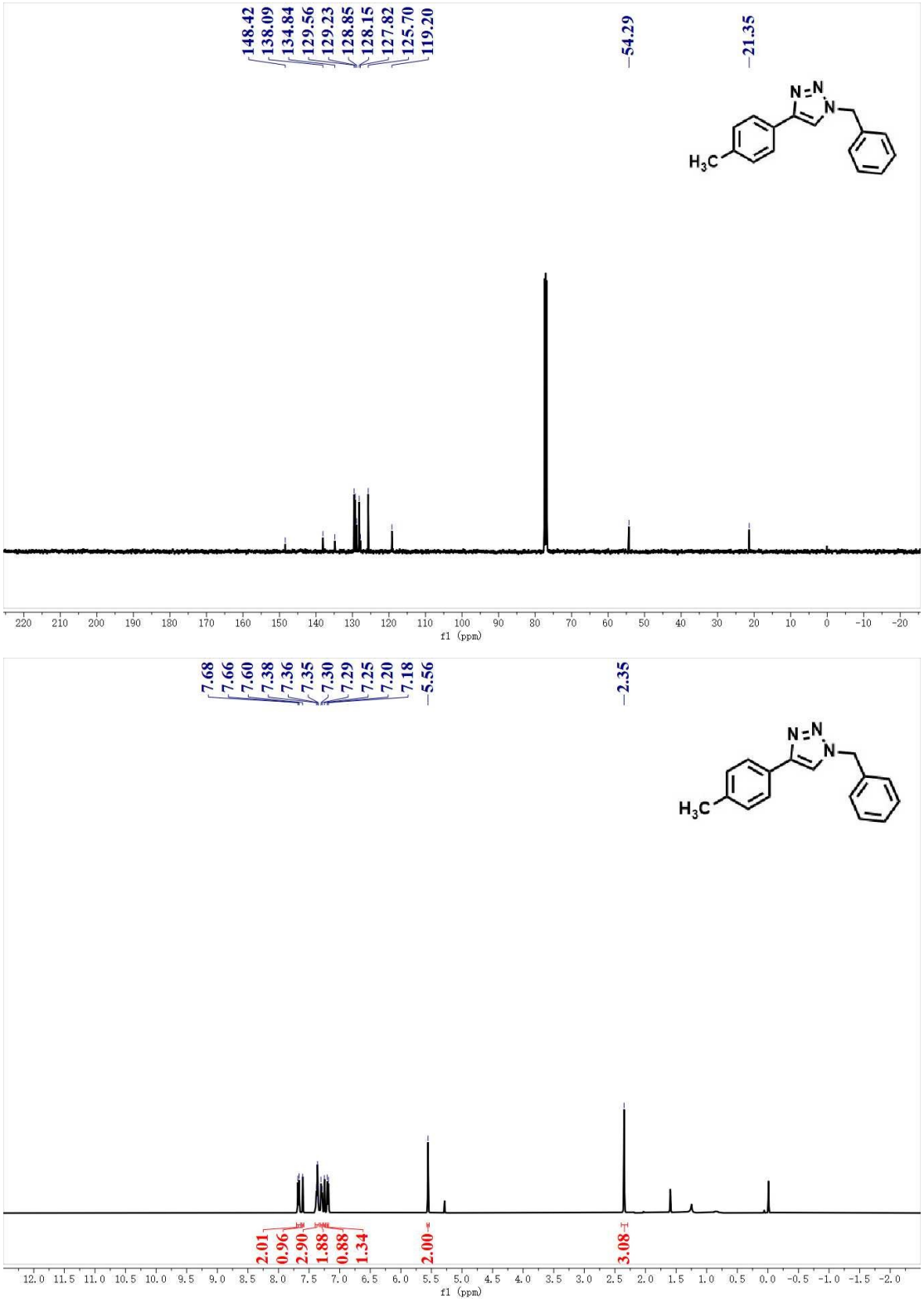

^{1}H and ^{13}C NMR spectra of 1-benzyl-4-(p-tolyl)-1*H*-1,2,3-triazole (in $CDCl_3$).

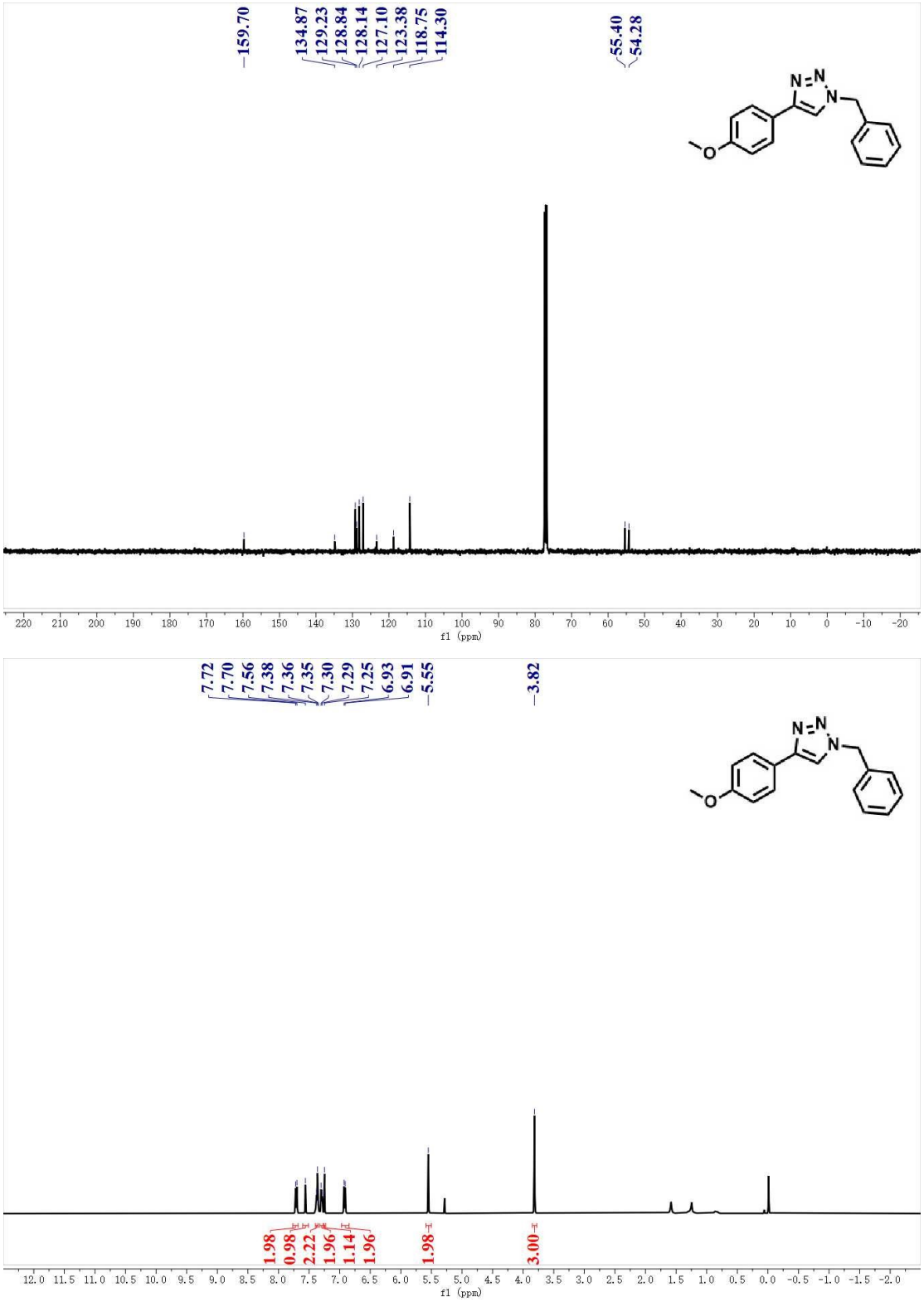

^{1}H and ^{13}C NMR spectra of 1-benzyl-4-(4-methoxyphenyl)-1*H*-1,2,3-triazole (in $CDCl_3$).

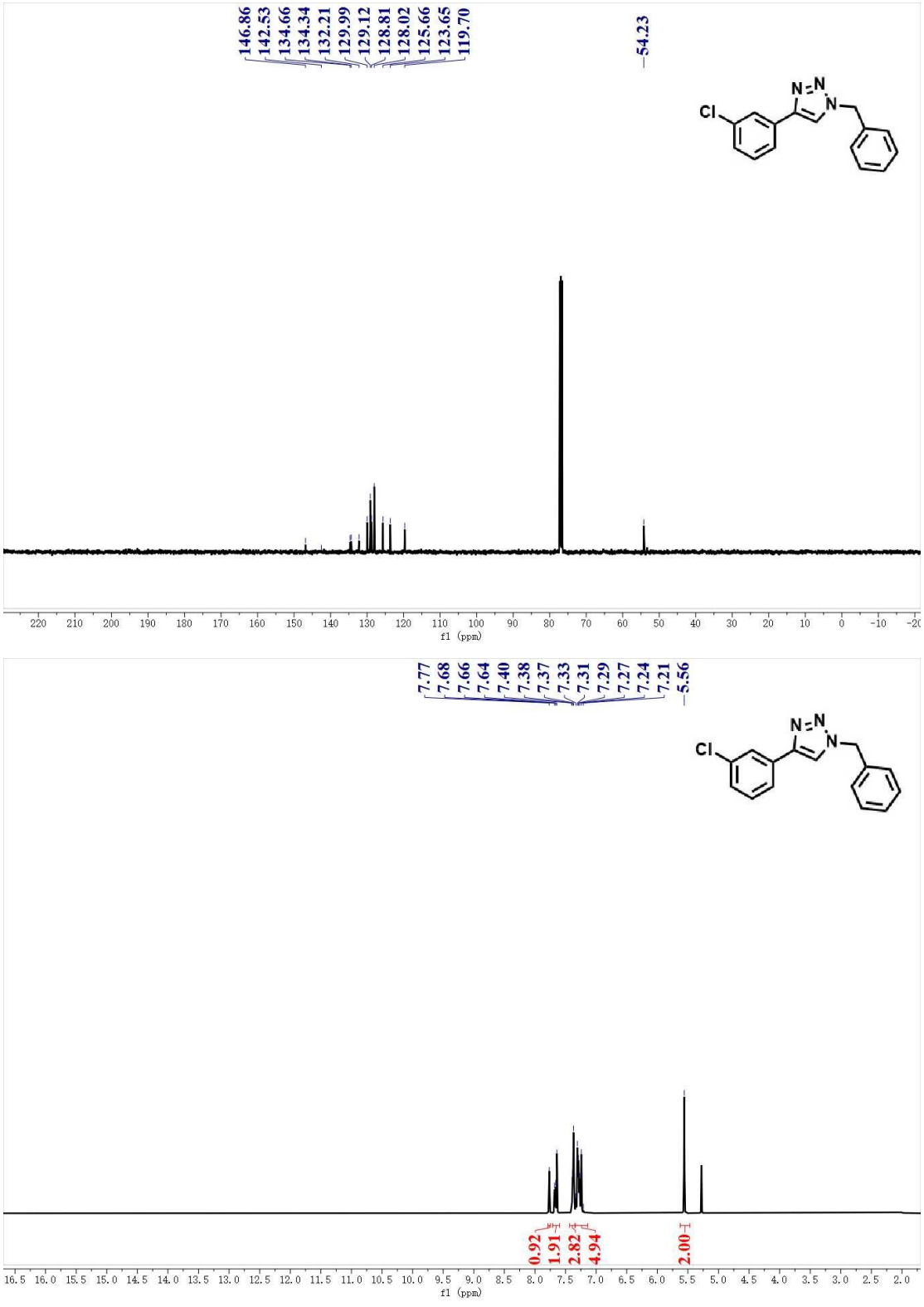

^{1}H and ^{13}C NMR spectra of 1-Benzyl-4-(3-chlorophenyl)-1*H*-1,2,3-triazole (in $CDCl_3$).

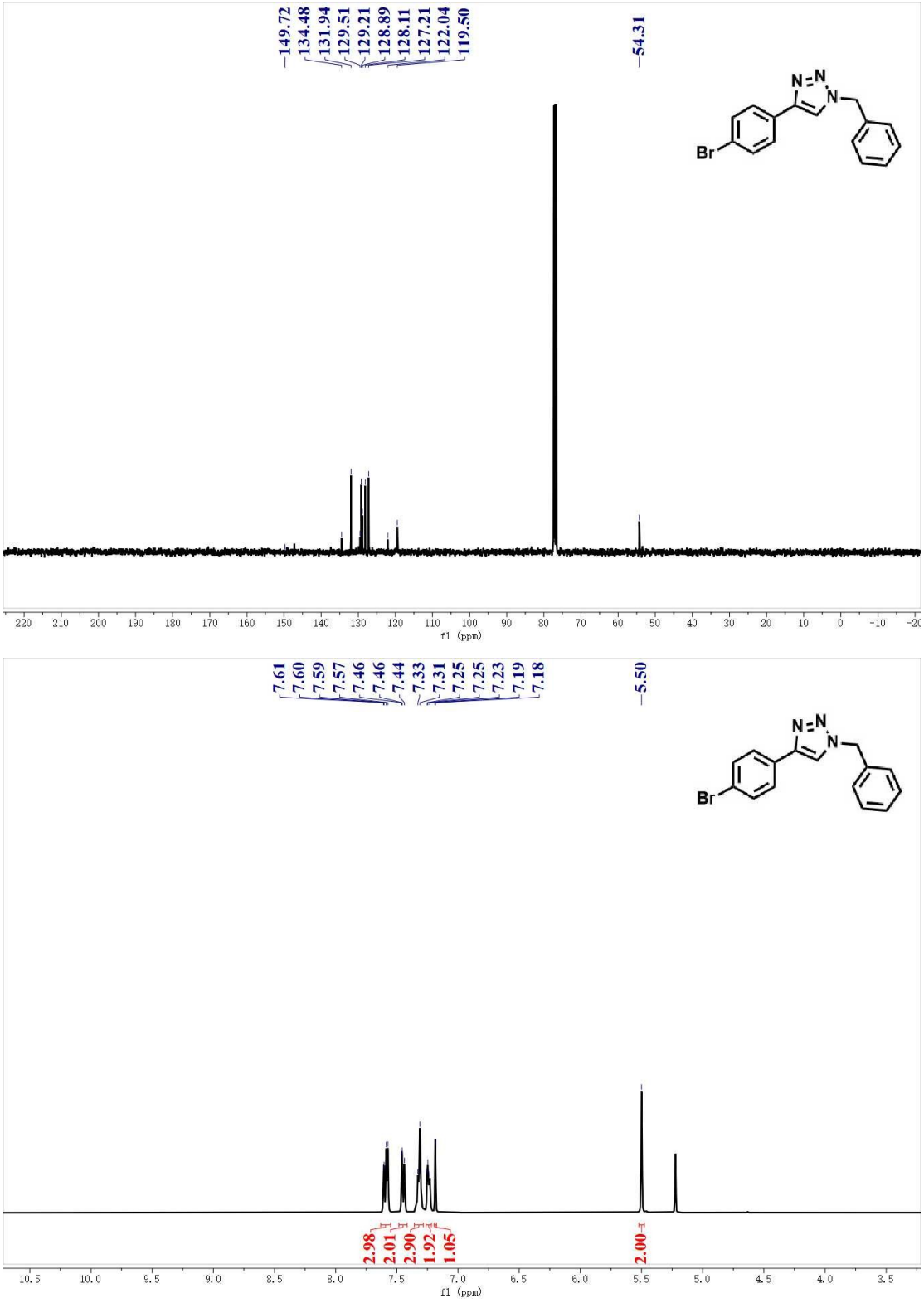

^{1}H and ^{13}C NMR spectra of 1-benzyl-4-(4-bromophenyl)-1*H*-1,2,3-triazole (in $CDCl_3$).

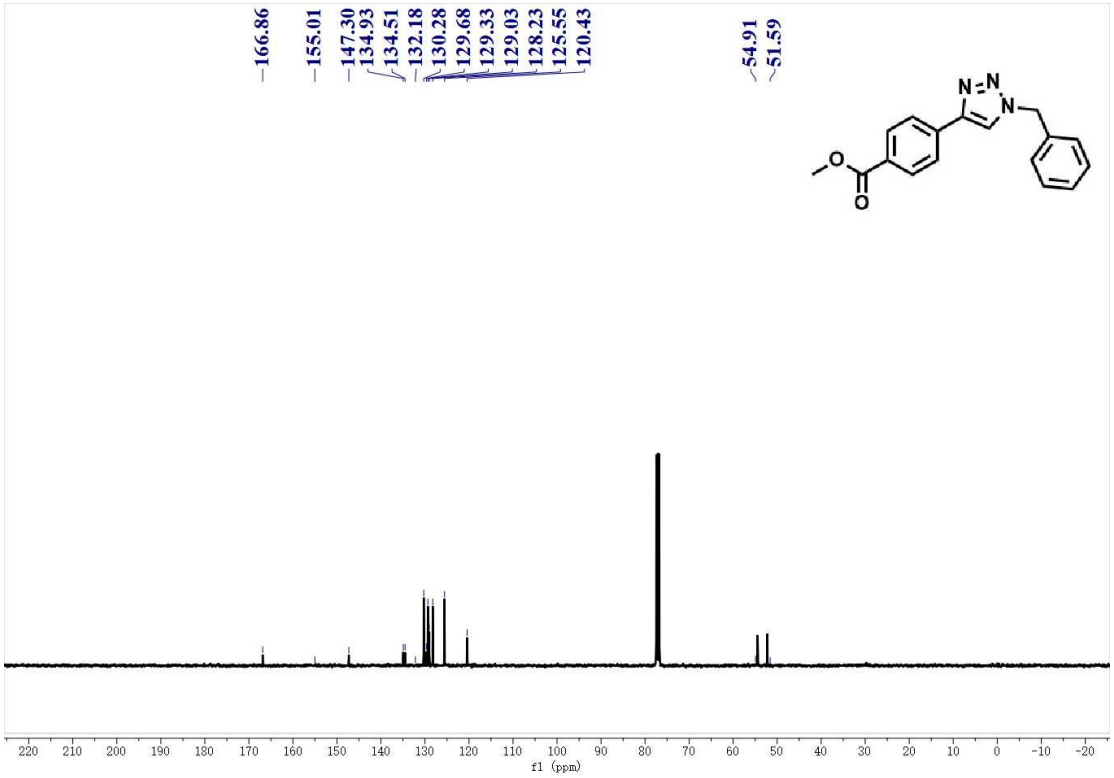

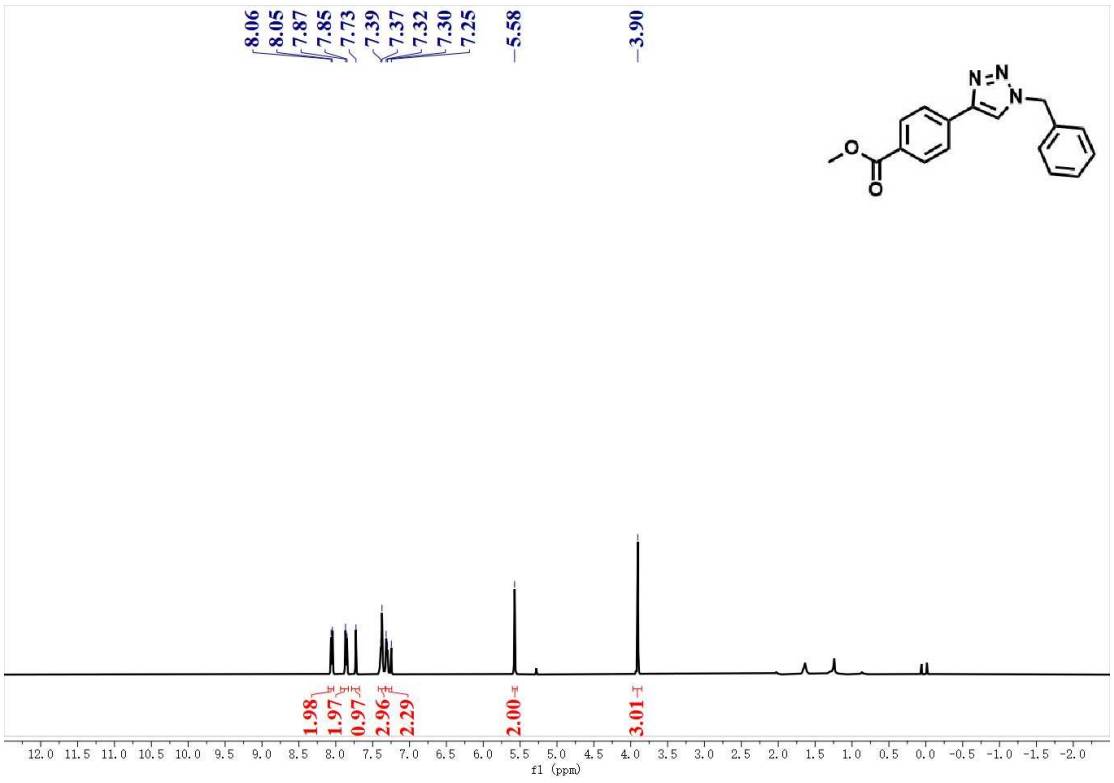

^{1}H and ^{13}C NMR spectra of methyl 4-(1-benzyl-1*H*-1,2,3-triazol-4-yl)benzoate (in $CDCl_3$).

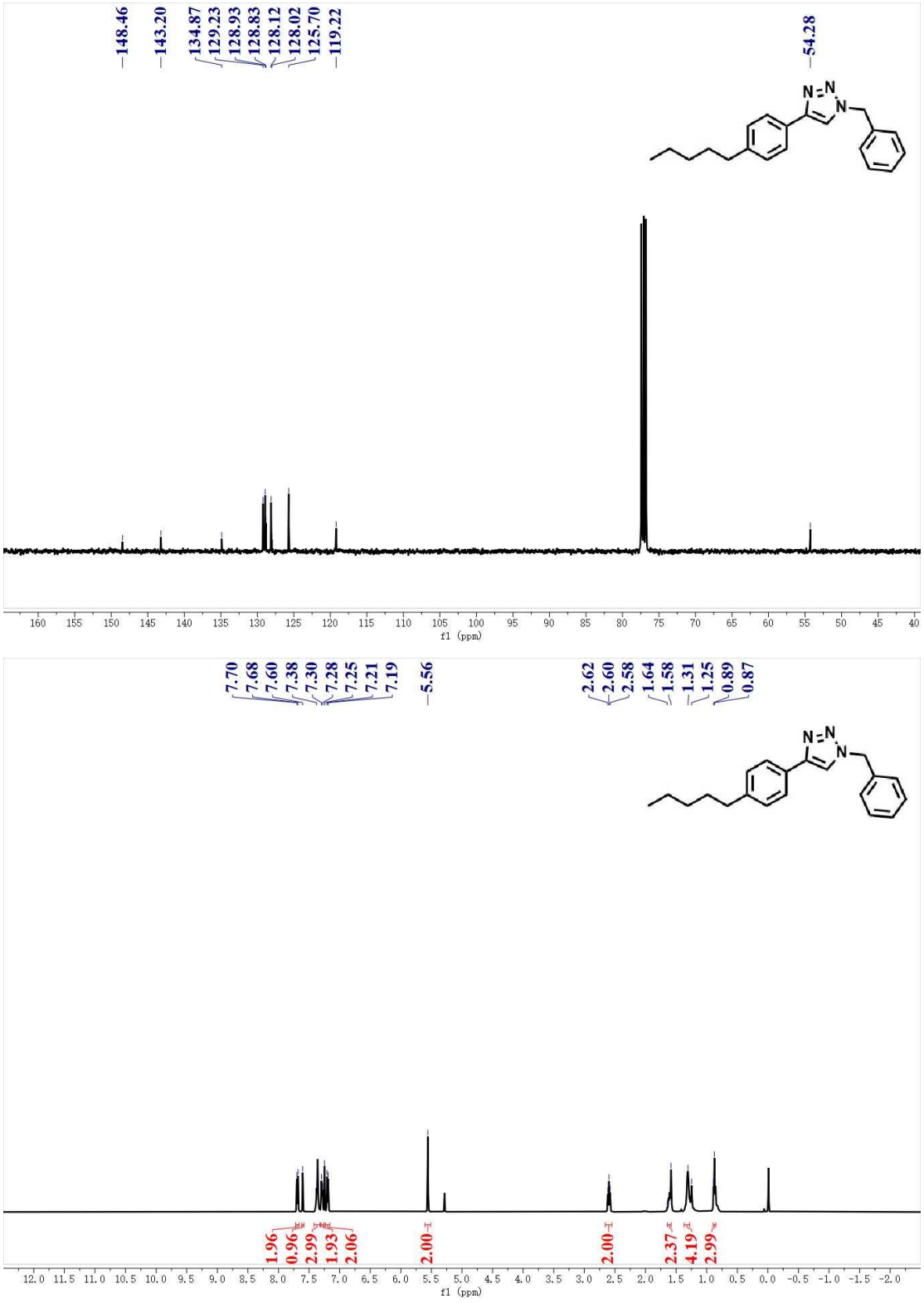

^{1}H and ^{13}C NMR spectra of 1-benzyl-4-(4-pentylphenyl)-1*H*-1,2,3-triazole (in $CDCl_3$).

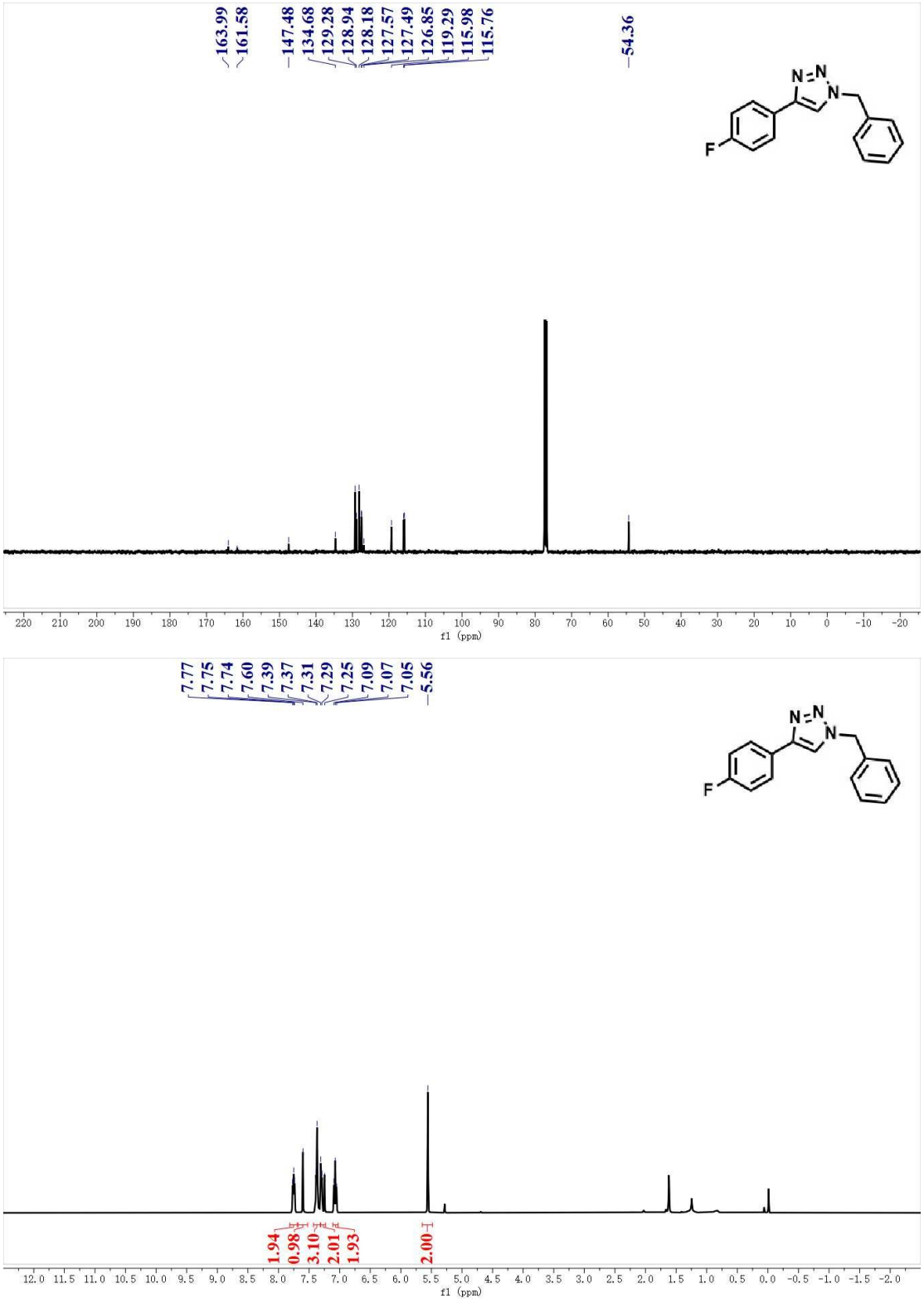

^{1}H and ^{13}C NMR spectra of 1-benzyl-4-(4-fluorophenyl)-1*H*-1,2,3-triazole ($CDCl_3$).

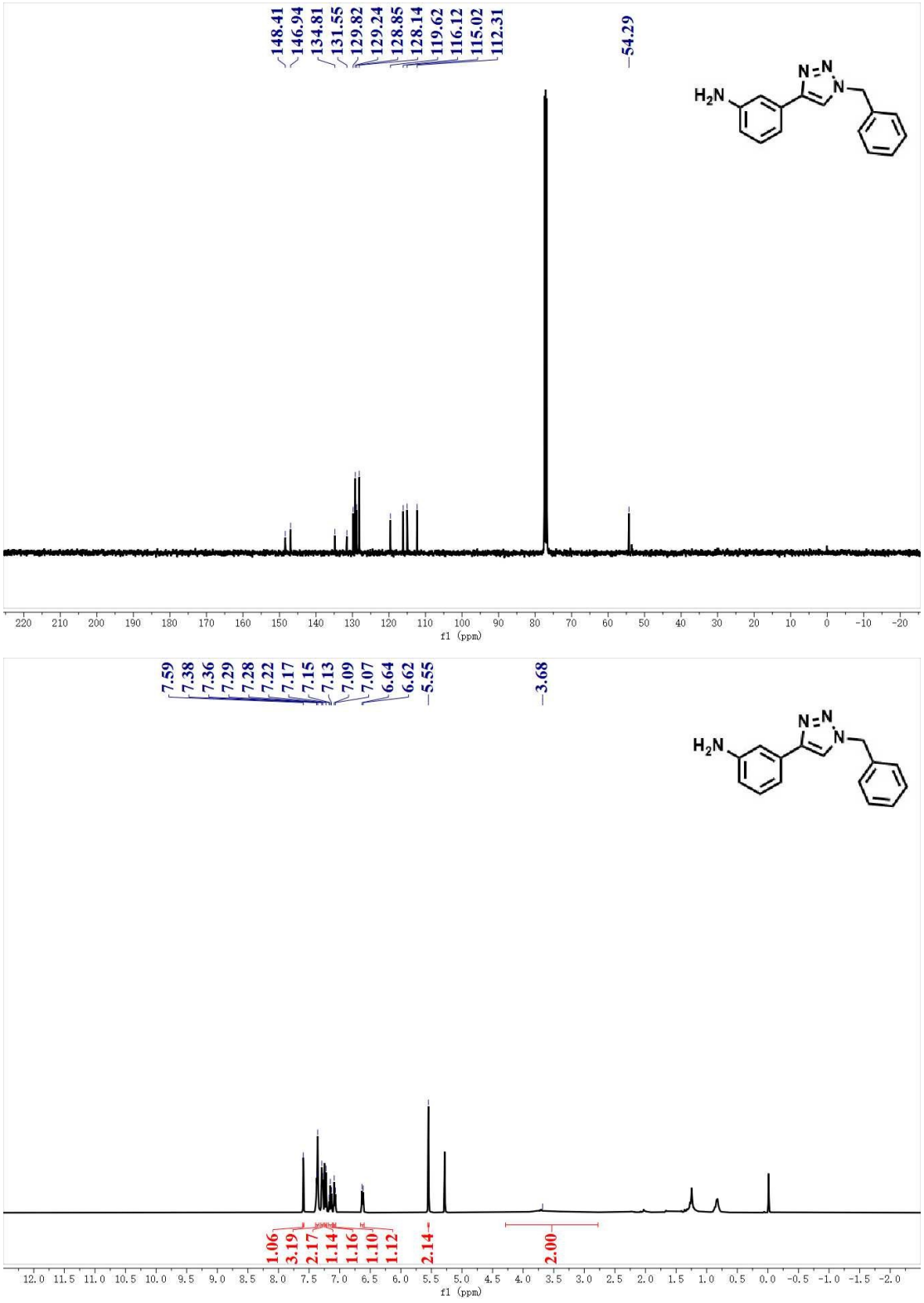

^{1}H and ^{13}C NMR spectra of 3-(1-benzyl-1*H*-1,2,3-triazol-4-yl) aniline (in $CDCl_3$).

References

1 Y. X. Mao, J. Cheng, H. Guo, L. Qian, Y. Xu, J. C. Tu, W. J. Yang, *Fuel,* 2023, **343**, 127848.

2 L. Chen, X. Kang, S. Jin, W. J. Du, S. X. Wang, M. Z. Zhu, *J. Phys. Chem. Lett.,* 2019, **10**, 6124-6128.

3 Z. Y. Chen, A. G. Walsh, X. Wei, M. Z. Zhu, P. Zhang, *Small,* 2021, **17,** 2005162.

4 J. L. Li, H. Li, H. Z. Yu, J. S. Chai, Q. Z. Li, Y. B. Song, Z. J. Zhang, M. Z. Zhu, *Dalton T.,* 2020, **49,** 7684-7687.

5 J. Z. Yan, H. F. Su, H. Y. Yang, C. Y. Hu, S. Malola, S. C. Lin, B. K. Teo, H. Häkkinen, N. F. Zheng, *J. Am. Chem. Soc.,* 2016, **138**, 12751-12754.

6 M. Madasu, C. F. Hsia, M. Huang, *Nanoscale*, 2017, ***9***, 6970-6974.

7 J. W. Wen, K. Wu, D. L. Yang, J. Tian, Z. Y. Huang, A. S. Filatov, A. Lei, X. M. Lin, *ACS Appl. Mater. Interfaces,* 2018, **10**, 25930-25935.

8 N. Li, X. Liu, *J. Chem. Res.,* 2020, **44**, 566-570.

9 D. S. Sá, E. J. Rodrigues, N. M. Suguihiro, A. G. Veiga, S. Paciornik, A. Massi, O. G. Pandoli, *Catal. Lett.,* 2022, **152**, 3558-3575.

10 P. Sharma, J. Rathod, A. P. Singh, P. Kumar, Y. Sasson, *Catal. Sci. Technol.,* 2018, **8**, 3246-3259.

11 G. Vilé, G. D. Liberto, S. Tosoni, A. Sivo, V. Ruta, M. Nachtegaal, A. H. Clark, S. Agnoli, Y. J. Zou, A. Savateev, M. Antonietti, G. Pacchioni, *ACS catal.,* 2022, **12**, 2947-2958.

12 P. Ren, Q. L. Li, T. Song, Z. Z. Wang, K. Motokura, Y. Yang, *ChemCatChem,* 2021, **13**, 3960-3966.

13 J. Pandey, B. D. Singh, H. Khanam, B. Tiwari, T. Azaz, R. Singh, *Int. J. Biol. Macromol.,* 2024, **255**, 128098.